Contact of Crack Surfaces during Fatigue: Part 1. Formulation of the Model

ANA MARÍA GARCÍA and HUSEYIN SEHITOGLU

A model has been developed to predict crack opening and closing behavior for propagating fatigue cracks which undergo significant sliding displacements at crack flanks. Crack surfaces were described statistically by assuming a random distribution of asperity heights and a mean density of asperities and asperity radii. The propagating crack was subdivided into strips, and each strip was treated as a contact problem between two randomly rough surfaces. The remote tensile stresses were varied in a cyclical manner. The contact stresses at minimal load were determined by analyzing the local crushing of asperities *via* a sliding mechanism. Then, upon loading, the crack opening stress levels were computed when the contact stresses were overcome. Part 1 of this article includes a discussion of the previous models, then introduces statistical contact mechanics concepts which are utilized in the fatigue crack growth simulations. In addition, the numerical algorithms for the modeling work and the sensitivity of results to model parameters are described. The role of stress ratio, maximum stress level, crack length, and the geometry of crack surfaces on the crack growth behavior will be discussed in Part 2 of this article.

I. INTRODUCTION

THE concept of crack closure has been universally applied to explain many observed fatigue crack growth behaviors, including R ratio effect, overload and underload effects in variable amplitude loading, material effects (yield stress, strain hardening, and slip behavior), maximum far-field stress, crack length, and geometry effects. Several investigators observed that crack growth behavior depends on the above factors even when plasticity effects (*i.e.*, plasticity-induced closure) are small. Crack roughness effects become dominant for coarse-grained and planar-slip materials near threshold or for small cracks driven under crystallographic slip, and can readily account for many of the observed crack growth behaviors. For an overview of the topic, the reader is referred to the textbook by Suresh[2] and the recent overview by Sehitoglu *et al.*[3] In many cases, the crack surfaces are not flat at the microlevel, and crack growth behavior is influenced by contact and sliding of crack surfaces. It is expected that the nonflat surfaces naturally arise due to slip planarity in metallic alloys and microstructural barriers and interfaces in metals and nonmetals. The interaction of such surfaces becomes complex and relevant to the characterization of crack growth behavior. The present work has undertaken the task of utilizing contact mechanics principles to determine crack opening stresses for crack surfaces ranging from rough to nearly flat. Such results have not been previously derived for crack profiles with statistical variation in heights of asperities and, ultimately, such a derivation could lead to better models for fatigue crack growth resistance. In this study, we will use the terms ''nonlinear crack path,'' ''irregular crack path,'' and ''nonflat cracks'' to indicate deviations of a crack from a straight path. The resulting crack closure is termed an ''asperity-induced closure'' or ''roughness-induced closure.'' ''Nominally flat'' surfaces are defined as appearing smooth at the macroscopic scale but having many asperities on them when observed at microscale or higher magnifications. This definition comes from the contact mechanics literature. For details of stresses in contacting bodies, the reader is referred to the book by Johnson.[4]

The mechanism by which the nonlinear crack paths contribute to crack closure has been well documented for the last 25 years. Early studies used the term crack ''roughness.'' Adams,[5] Purushotham and Tien,[6] and Walker and Beevers[7] were the first to note the role of roughness and closure of cracks at discreet points behind the crack tip. Davidson and Lankford[8] measured substantial mode II displacements under far-field mode I loading conditions when studying crack growth in 7075 Al alloys. In their investigation, the mode II displacements exceeded mode I displacements near the crack tip. These and other experimental investigations suggested that during a fatigue cycle, mode II displacements develop around the crack tip if the crack faces are not flat.[9] As the crack faces are displaced in the direction parallel to the crack growth, they undergo contact stresses which could exceed the yield strength of the material. When far-field loading is increased in the tensile direction, these stresses have to be overcome before the crack can advance. This particular mechanism, crack closure with local sliding, has been used to explain microstructurally sensitive fatigue crack growth behavior, particularly in the near-threshold regime. Crack opening stresses in the presence of nonflat crack surfaces can be as high as 0.9 of the maximum stress. Since plasticity-induced closure cannot produce such high crack opening stresses, the majority of closure contribution is attributed to the nonflatness of the cracks. As the crack growth rates increase, the crack opening stress levels decrease gradually. The present study attempts to study the role of asperity-induced closure in an attempt to isolate this type of closure contribution.

Numerous investigations postulated, based on crack

ANA MARÍA GARCÍA, Research Assistant, and HUSEYIN SEHITOGLU, Professor and Associate Head, are with the Department of Mechanical and Industrial Engineering, University of Illinois, Urbana, IL 61801.

Manuscript submitted March 5, 1997.

growth trends, that plasticity-induced closure effects in the near-threshold regime are small compared to crack surface interference effects. At low stress intensities, primarily plane strain conditions exist, and the effect of the plastic wake and crack tip plasticity may be negligible since the plastic zone ahead of the crack tip (responsible for plasticity-induced crack closure) is small. Also, the anisotropic character of the material at this size scale leads to growth with planar slip and, consequently, to nonlinear crack paths. These observations led to the conclusion that roughness effects are the main closure mechanism in the near-threshold regime. Roughness effects are significant in titanium alloys with different slip characters[10,11] and steels with lamellar microstructures (prior austenite grain size and pearlite spacing.[12] Nickel based superalloys[13] and aluminum alloys[14,15] undergoing planar slip and titanium aluminides with lamellar and duplex microstructures also exhibit nonlinear crack paths. More details of the experimental work will be provided in Part 2 of this article.[1] Materials and conditions which produce crack paths deviating from a straight crack front exhibit superior fatigue crack growth resistance in the threshold regime. This opens the possibility of designing alloys with better performance compared to conventional alloys.

Since the early 1980s, several fatigue researchers have correlated the roughness dimension, the material microstructure, and the fatigue crack growth resistance of a material near the threshold. Few models have been forwarded to capture the crack deflection on crack growth rates. Periodic tilting has been analyzed by Suresh[16] using the local driving-force calculations associated with kinked cracks.[17] In the case of deflection of a tensile crack from the nominal modeI plane, mixed-mode crack tip conditions develop, and these can be handled in the context of fracture mechanics without invoking crack closure concepts. Suresh and Ritchie[18] proposed a closure model which predicts the role of mode II (or sliding) displacements. In a later work, Smith and Smith[19] noted the locking of asperities and gross plastic deformation of asperities, but they have not analyzed the contact stresses.

The discrete asperity contact has been analyzed by a number of investigators. Nakamura and Kobayashi[20] idealized the crack surface with long strips to simulate asperities. They examined the location of the asperities with respect to the crack tip and showed that asperity-induced closure raises the crack opening stress to near 0.8 S_{max}. Since their model is based on plane stress, it does not capture the plane strain deformation typically observed near threshold. Beevers *et al.*[21] analyzed a single asperity behind the crack tip and showed that the location and rigidity of the asperity influenced closure. But this is not sufficient to accurately describe the interference of many asperities over the entire crack face. In cyclic loading conditions, the interference of crack surfaces occurs over the entire crack length with hundreds of contact points, and a general model has not emerged that addresses this condition. In Beevers' work, the effect of oxide debris was also included by treating it as asperities. It is worth noting that in titanium alloys, oxide thicknesses near 1 μm were measured by Allison and Williams[10] and have a diminishing role if the asperity heights exceed this dimension. These models did not address the contact stresses associated with asperity interference in the transverse direction. Previously, when the problem was geometrically formulated, no load transfer was analyzed, and the local plastic flow and effect of material properties were not fully accounted for. The contact mechanics associated with sliding of asperities over each other present modeling challenges which will be addressed in this work.

In a finite-difference study, Llorca[22] idealized the crack profile by predefining a triangular crack surface shape. He predicted normalized closure levels in the range of 0.4 to 0.62 for asperity heights near 10 μm. This calculation is in accordance with the model in this work (Part 2 of this article[1]) and experimental results on Al 2124. The finite-difference and finite element model techniques are powerful, but because of excessive computer times, it is difficult to achieve a full representation of surface topography with these models.

Several simple models predict the effect of multiple asperities[23] between the two surfaces and friction.[24] The recent model of Tong *et al.* also studied the role of mode II displacements and inclination angles. These models are useful, but they use linear relationships between contact load and crack surface displacement. This relationship should be nonlinear for two reasons: first, as the crack surfaces are pressed, the contact area increases nonlinearly with load (even under elastic compression of asperities), and second, the crack surfaces in ductile metals undergo plastic deformation (which is inherently three-dimensional in contact problems). Therefore, the aforementioned models should be considered geometric in nature.

In light of the relevance in the development of improved fatigue crack growth models, the current article focuses on modeling the contact of nonflat crack surfaces. The present development characterizes the crack surface interaction by employing a statistical description of contact, common in the study of wear, to analyze rough fracture surfaces. The crack was subdivided into a number of strips, and this discretization treats each strip as a contact problem of two surfaces with asperities. The asperities can be characterized by an average tip radius, a random distribution of heights, and a density (*i.e.*, number of asperities per unit length). The current model can handle various R ratios, maximum stress levels, crack lengths, and topographical features that could not be as readily treated in previous research. The current work will assume that the magnitude of the mode II displacements near the crack tip are sufficient to constitute sliding (*i.e.*, one asperity passes another). Thus, at the individual asperity level, the problem is treated as a two-dimensional plane strain sliding contact. Sliding and plastic flow of asperities occurs at length scales comparable to microstructural dimensions; however, as a first approximation, we will assume isotropic, homogenous material.

The main features that we aim to uncover in this article include an examination of different models for the study of the contact of two nonflat surfaces, a detailed description of the proposed crack closure model and some of the assumptions made, the influence of the geometrical description of crack surfaces (Gaussian *vs* exponential distribution of heights) on crack opening stress, the influence of plastic flow at the asperity level on crack opening stresses, and the sensitivity of the number of strips on crack opening stress.

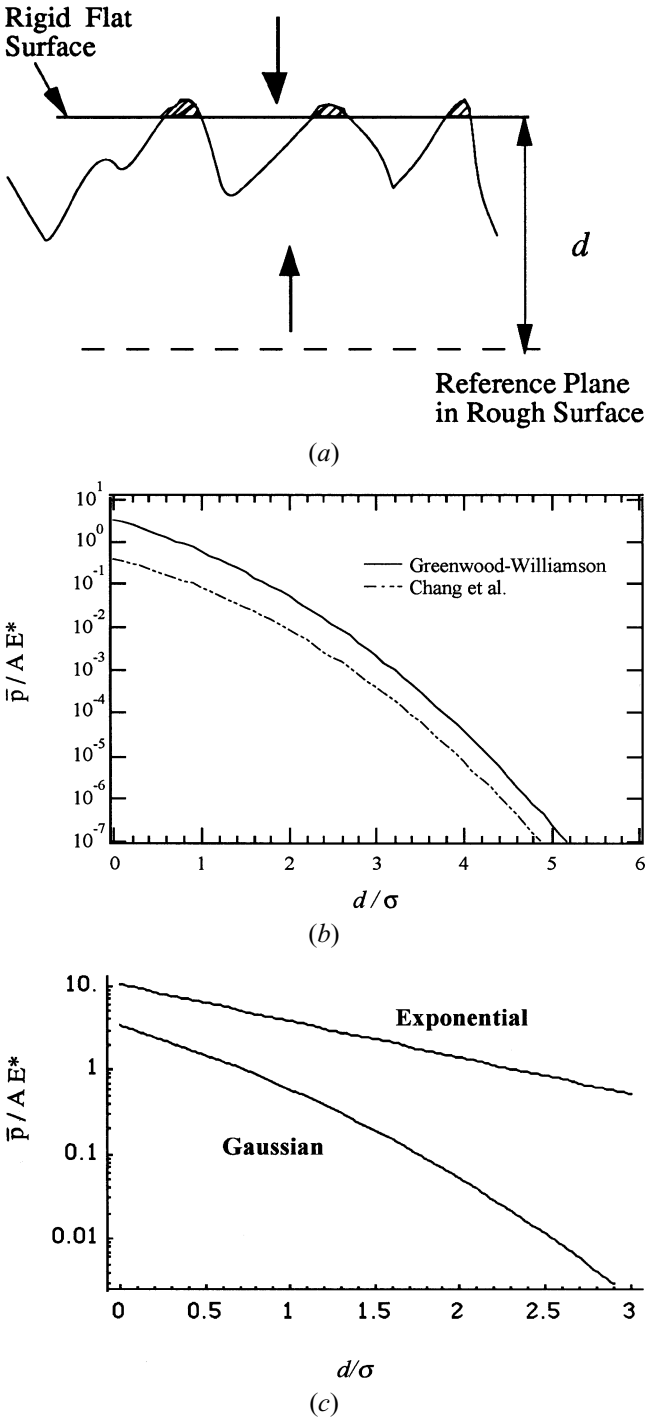

Fig. 1—(*a*) Schematic of rigid flat surface and nonflat surface containing asperities. (*b*) Comparison of load-separation distance relationship for a constant asperity density for two models. In these cases, $\sigma = 46\ \mu$m, $R_e = 1/250$ m, $N = 3{\cdot}10^6$ asperities/cm, $E = 180$ GPa, and $S_y = 450$ MPa.(*c*) A comparison of load-displacement relationship for the exponential and Gaussian distribution heights (GW model; $\sigma = 46\ \mu$m, $R_e = 1/250$ m, $N = 3{\cdot}10^6$ asperities/cm, $E = 180$ GPa, and $S_y = 450$ MPa).

II. DEVELOPMENT OF THE MODEL

A. *Models of Contact between Nominally Flat Surfaces*

As aforementioned, individual ''strip events'' (or strips) were modeled as two nominally flat surfaces under repeated normal contact. This local characterization is based on the statistics of a rough surface. Greenwood and Williamson (GW)[25] first developed this statistical approach to study the elastic contact of two nominally flat surfaces which are pressed together by a normal load. Subsequent contact models have modified the GW original model in the choice of unit event or the behavior of the individual asperities, but the statistical description remains the same. In the present work, before we chose a unit event, it is instructive to review the GW analysis to model the strip event.

Greenwood and Williamson[25] considered the case of elastic contact between a randomly rough surface covered with rounded asperities and a rigid flat surface. The first step was to choose an appropriate ''unit event'' which described the behavior of a single asperity. In their case, the Hertzian contact equations were appropriate. Thus, the load on a single asperity (P) is given by

$$P = \frac{4}{3} E^* R_e^{1/2} \Delta_o^{3/2} \qquad [1]$$

where R_e is the radius of the sphere which comes in contact with the plane, E^* is the plane strain modulus ($E^* = 2\left(\frac{E}{(1-\nu^2)}\right)$), and Δ_0 is the compliance or normal displacement due to the local compression.[26]

The rough surface is statistically characterized by a random distribution of heights, constant asperity tip radius, and a density of asperities. A Gaussian distribution of heights has been shown to describe the contacting surfaces; therefore, it has been chosen initially. The role of other distributions will be discussed later. By defining the probability of asperities making contact, the load carried over a randomly rough surface which results from the collective elastic compression of many asperities was calculated. As noted earlier, a random surface pushed against a rigid flat surface is analyzed (Figure 1(a)).

The statistical analysis follows, for the most part, GW's original work. The heights on a surface vary randomly, and the probability that a particular asperity has a height between z and dz is given by a probability density distribution $\Phi(z)dz$. Then, if two surfaces, only one of them being rough, come together until their reference planes are separated by a distance d, there will be contact at any asperity whose height is greater than d. Therefore, the probability of making contact for an asperity of height z is given by

$$\text{prob}\ (z \geq d) = \int_d^\infty \Phi(z)dz \qquad [2]$$

where d is the distance that separates the two surfaces and z is the height of an individual asperity. If N is the total number of asperities, then the number of asperities in contact is given by

$$n = N \int_d^\infty \Phi(z)dz \qquad [3]$$

The compliance can be written as

$$\Delta_o = z - d \qquad [4]$$

Therefore, using this expression, we can incorporate the unit event into the statistics of contact for the surface and

obtain an expression for the total load in terms of the separation distance:

$$\overline{p} = \frac{4}{3} N \cdot E^* \cdot R_e^{1/2} \cdot \int_d^\infty (z - d)^{3/2} \cdot \Phi(z) \cdot dz \quad [5]$$

Two distributions of $\Phi(z)$ have been used. If the reference plane from which the asperity heights are measured is at the mean, then a Gaussian or normal distribution is given by

$$\Phi(z) = \frac{1}{\sigma\sqrt{2\pi}} \exp\left(\frac{-z^2}{2\sigma^2}\right) \quad [6]$$

and the exponential distribution is given by

$$\phi(z) = \frac{1}{\sigma} \exp\left(\frac{-z}{\sigma}\right) \quad [7]$$

where σ is the standard deviation of asperity heights.

The separation distance is d, and the load-separation distance ($\overline{p}/A\ E^*$ *vs* d/σ) relationship which results from this analysis is presented in Figure 1(b). Note that this is a log-linear plot. The load-displacement relationship is nonlinear, because as the surfaces are pressed together, the real contact area increases nonlinearly as the asperities contact gradually. In this figure, $\overline{p}$ is the total normal load, A the nominal contact area, E^* the plane strain elastic modulus, d the separation distance, and σ is the effective standard deviation of heights. Note that $\overline{p}$ is the summation of all the single-asperity contact loads P (given as Eq. [1]). We assumed a normal distribution of asperity heights and that no permanent deformation occurs in the GW model. The total normal load obtained for the case of Gaussian and exponential distribution of heights is compared in Figure 1(c). The exponential distribution of heights requires higher loads for the same separation distance of crack surfaces. The simulations for these cases are conducted for given average asperity heights, asperity densities, and asperity radii, which are noted in the figure.

Greenwood and Tripp[27] later modified the GW analysis to account for the misalignment of asperities of two rough surfaces. However, they concluded that in the context of *elastic* contact the contribution of the misalignment is not, for all practical purposes, significant. The GW model was further modified by Chang *et al.*[32] to include plastic flow in the context of perfect plasticity. The load-separation distance ($\overline{p}/A\ E^*$ *vs* d/σ) relationship was modified, and is also shown in Figure 1(b). The material properties used for the simulation are indicated in the figure. A normal distribution of asperity heights was assumed to exist before any permanent deformation occurred. As the surfaces separate $d/\sigma > 5$, the contact loads decrease considerably. As d/σ approaches zero, the surfaces adhere and maximum contact loads are predicted. Note that the contact load-displacement relationship is nonlinear in both cases. Since the crack surfaces undergo substantial sliding, we next consider the sliding deformation of asperities.

B. *Normal Load vs Crushing Distance for Two Asperities*

In an effort to construct a GW-type model for the study of crack surface contact, the Johnson–Shercliff (JS)[28] analysis of individual asperities under repeated sliding contact was chosen as a unit event. The unit event for sliding of asperities is shown in Figure 2(a). Two asperities with radii R_1 and R_2, respectively, undergo maximum deformations of Δ_{01} and Δ_{02}, respectively. Their analysis leads to the load-normal displacement relation in Figure 2(b), which is analogous to the Hertzian load-compliance relationship (Eq. [1]) employed in GW's work. The symbols in Figure 2(b) will be explained in detail subsequently. It was assumed by JS that, after repeated sliding, plastic flow occurs and conditions may be such that in the steady state, shakedown is achieved and elastic deformation follows. In this context, they described the individual asperity behavior for two cases: contact of a soft and a hard asperity and contact of asperities of equal hardness. For contact of crack surfaces, the second case is relevant.

This unit event problem (Figure 2(a)) is one of plane strain deformation of rounded asperities with their axes perpendicular to the direction of sliding. The contacting asperities are viewed as two cylindrical bodies pressed in contact by a normal force per unit thickness (P). This force can be interpreted as the normal load which results in a compression Δ_0, the initial interference at a position x in a contact path. Note that $\Delta_0 = z - d$. If the asperities are assumed to undergo uniform contact stresses across the entire encounter, the steady-state asperity profile can be predicted. This also leads to an expression for the total load carried over the encounter, dependent only upon material properties and the *initial* (undeformed) asperity geometry.

The JS model determined the mean load over an encounter by separately analyzing the initial elastic asperity encounter and the steady state (shakedown). During the encounter, the contact starts at the leading edge; the contact pressure rises and reaches a maximum at the crest point, then decreases. Since we are interested in the average load, the average load over the entire encounter at shakedown ($\overline{P}$) is obtained by integrating the load carried at a static stage of contact during the sliding ($P(x)$) over the half-contact path (x_m):

$$\overline{P} / R_e E^* = \int_0^{x_m} (P / R_e E^*) dx \quad [8]$$

where R_e is the effective asperity tip radius and E^* is the plane strain elastic modulus. It was assumed that at the shakedown state, the shakedown pressure (p_0^s) for existing shear traction conditions remains constant throughout the contact period. That led to the following expression for the mean load per unit length carried over an encounter by two asperities of equal hardness:

$$\frac{\overline{P}}{R_e E} = \pi\left[\frac{p_o^s}{R_e E}\right]^2 \frac{\delta_o}{\Delta_o}\left[\frac{\Delta_o}{R_e C}\right]\frac{1}{\sqrt{2}} \quad [9]$$

where Δ_0 is the initial interference between asperities, δ_0 is the interference at shakedown, and C is a nondimensional constant dependent on material properties (p_0^s and E^*) by $\left[\frac{p_0^s}{E^*}\right]^2 [2 \ln (4\ E^* / p_0^s) - 1\ ]$. The term p_0^s is the contact pressure at shakedown. It can be obtained from the shakedown map for steady sliding of two cylinders. This map is illustrated in Figure 2(c).[4,28] The geometry of the contact is also shown in the right-hand figure in Figure 2(c). In this

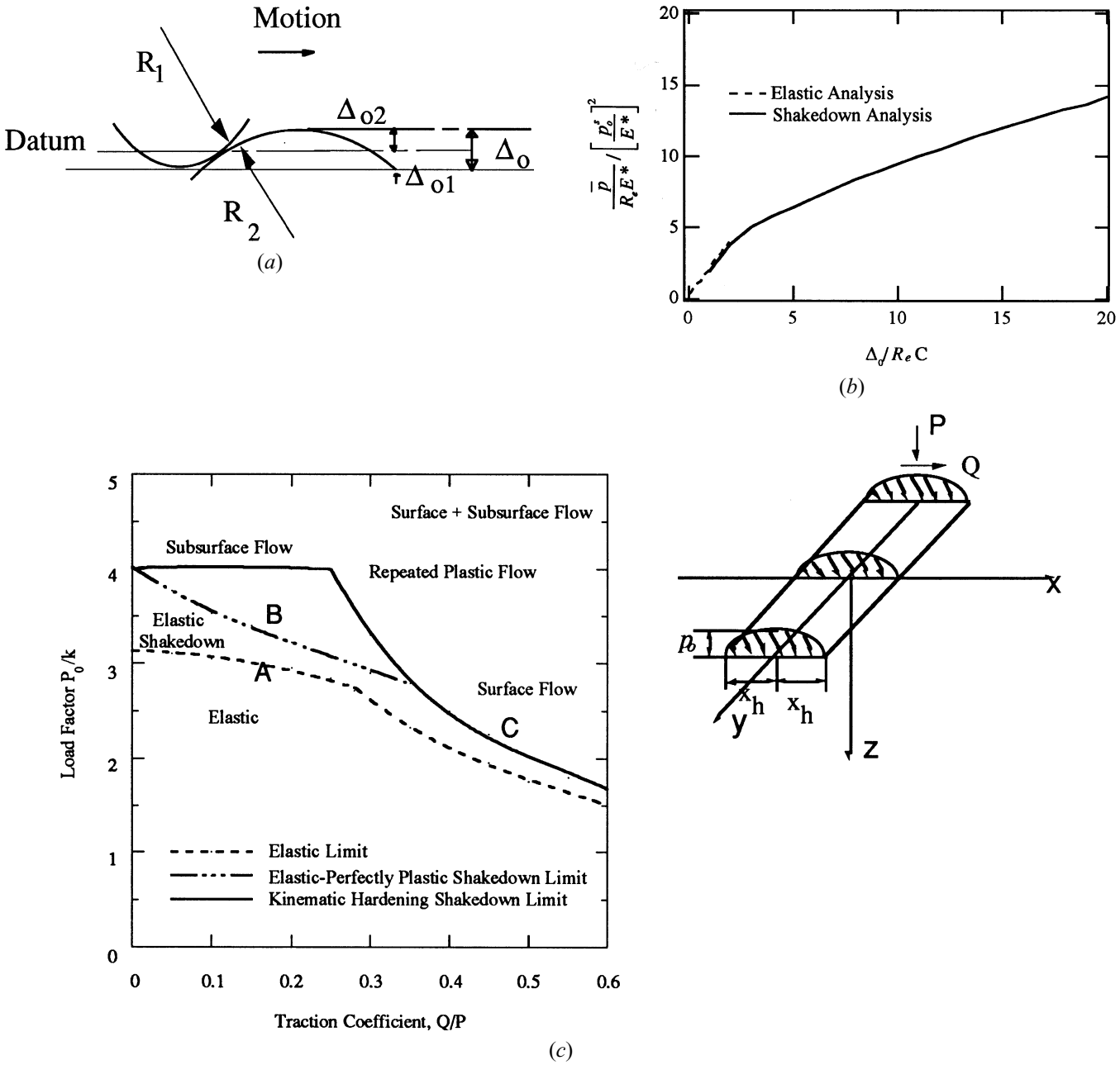

Fig. 2—(*a*) Schematic of sliding contact between two asperities (unit event). (*b*) Normalized load $\frac{\bar{p}}{R_e E^*} / \left[\frac{p_0^s}{E^*}\right]^2$ *vs* interference curve for two asperities in sliding contact. (*c*) Shakedown map for plane strain contact in half-plane and the geometry of contact.

figure, x is the crack growth direction and y is the thickness direction. The Hertzian pressure integrated over the contact width $2x_h$ results in the total normal load (P) and shear load (Q). The applied contact stress factor is defined by p_0/k, where p_0 is the peak pressure in Hertzian contact (which has the elliptical shape) and k is the yield stress in shear. Curve B is the shakedown limit (p_0^s) for elastic–perfectly plastic material. It is higher than the elastic limit (shown in curve A), especially at small values of traction coefficient. In this case, the material will yield in the first loading but then becomes elastic in subsequent loadings. Shakedown is achieved because the profile of the asperities is modified under the plastic flow and, in the limits of the contact region, experiences a constant shakedown pressure (p_0^s/k) during the contact period. In the analysis of Johnson and Schercliff,[28] the shakedown limit shown in Figure 2(c) was assumed to hold between the two asperities. Clearly, if the geometry of contact changes from the cylindrical plane strain contact situation used in derivation of Figure 2(c), the results need to be modified.

The tangential-to-normal load ratio (Q/P) enters the analysis because it changes the shakedown pressure to shear yield stress ratio (p_0^s/k) along curve C. This ratio depends on the choice made for the shakedown map. This, in turn, is dependent on the geometry of the unit event problem. The simulations were conducted for two cases. In the first case, $p_0^s/k = 4.0$, corresponding to a traction coefficient of zero. However, when shear tractions were present ($Q/P >$

0), then the value of p_0^s/k decreased to a value less than 4.0. Therefore, for the second case, the value $p_0^s/k = 2.5$ was used, which corresponds to a traction coefficient (Q/P) of 0.4.

It is assumed that the asperities change their profile to assume the constant value of p_0^s. The shakedown pressure is higher than the initial pressure to reach the elastic limit, because, as deformation progresses, residual stresses develop that raise the elastic limit in subsequent loadings. The concept of shakedown will be discussed in more detail in Part 2 of this article.[1] If it is assumed that the displaced material from the crests of the sliding asperities appears in the downstream bulge, then δ_0/Δ_0 is a function of the initial interference, undeformed asperity geometry, and material properties. This relationship is given by

$$\frac{\delta_o}{\Delta_o} = X_m\sqrt{\frac{4R_eC}{\pi\Delta_o}} \qquad [10]$$

where $X_m = x_m/x_e$, the ratio of the half-path length of contact at shakedown to the half-path length of elastic contact, and can be obtained by solving the equation

$$3\sqrt{\frac{2}{\pi}}\left[\frac{R_eC}{\Delta_o}\right]^{1/2} X_m^2 + \frac{1}{2}[(2X_m - 1)^2 - 1]^{3/2} + \frac{1}{2}(2X_m - 1)^3 - \frac{3}{2}(2X_m - 1) - 1 = 0 \qquad [11]$$

This is a nonlinear equation which is solved using Mathematica software. Therefore, the total load carried over the encounter is dependent only on material properties (p_0^s and E^*), the initial (undeformed) radii (R_e), and interference (Δ_0).

In Figure 2(b), the normalized load is plotted in the y-axis. In the x-axis, the normalized initial interference is given. This normalization permits applicability to any material. The elastic analysis is valid up to the elastic limit prescribed by the shakedown map of two individual asperities, which corresponds to $(\Delta_0/R_eC) = 0.1$. It is noted that this portion of the curve is linear, as expected. The shakedown portion is valid from $(\Delta_0/R_eC) = 1$ on. The gap between the two regions corresponds to the portion of the sliding encounter where the asperities flow plastically before achieving shakedown. The behavior in this region has been determined by extrapolating the curves that correspond to the shakedown and elastic analysis. The analysis conducted here follows JS's work considering asperities of equal hardness.

C. *Normal Load vs Separation Distance Relationships*

In the current work, the Kapoor and Johnson (KJ)[29] model was modified by employing an equal hardness unit event and by accounting for the statistics of *two* randomly rough surfaces in contact. The geometry is shown in Figure 3(a). Each surface is characterized by an initial asperity height distribution, a constant asperity tip radius, and a constant density of asperities. The present model assumed that all surfaces present a Gaussian distribution of heights and that contacting surfaces have the same standard deviation of height, radius, and density of asperities.

The KJ model used the hard-on-soft asperities unit event to study the problem of one randomly rough surface in sliding contact with a nondeforming one. In this case, the nondeforming asperities had constant radii but varying heights. Unlike the elastic-plastic static analyses mentioned earlier, their model accounted for change in asperity profile over cycling and its effect on the statistics of the surface. In this case, the normal load results from the integration of the stresses corresponding to the unit event load over a sliding encounter. Therefore, the total *normal* load ($\bar{p}$) over the entire sliding encounter, in the absence of tangential traction ($Q/P = 0$), is established. The results for this case are shown as Kapoor–Johnson in Figure 3(b).

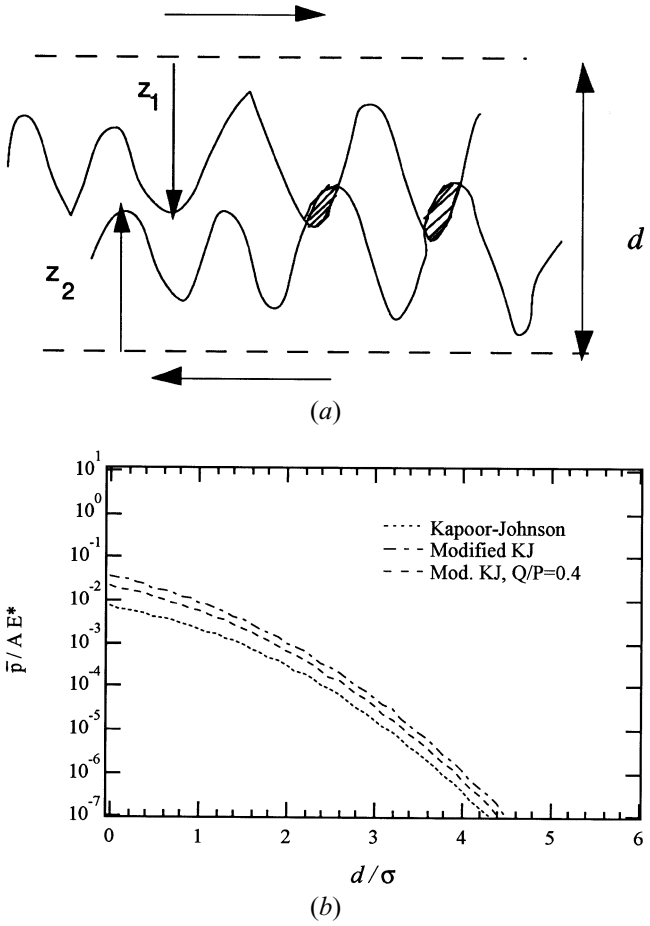

Fig. 3—(*a*) Schematic of randomly rough surfaces undergoing sliding. (*b*) Comparison of load-separation distance relationship for a constant asperity density for four models proposed. In these cases, $\sigma = 46$ μm, $R_e = 1/250$ m, $N = 3{\cdot}10^6$ asperities/cm, $E = 180$ GPa, and $S_y = 450$ MPa.

If two surfaces are pressed together, one of them being randomly rough and having a probability density function ($\Phi(z)$), then the probability of contact is given by

$$\text{prob}\ (z \geq d) = \int_d^\infty \Phi(z)dz \qquad [12]$$

In the case of two randomly rough surfaces, contact will occur when the sum of the asperity heights $z_1 + z_2$ exceeds the separation distance (d). Therefore, the probability of contact between randomly rough surfaces is given by

$$\text{prob}\ (z_1 + z_2 > d) = \int_d^\infty \Phi(z_1 + z_2)d(z_1 + z_2) \qquad [13]$$

Assuming that both surfaces are normally distributed and have a standard deviation σ, thus, $\Phi(z_1 + z_2)$ is also normal with standard deviation $\sigma = \sqrt{2}\sigma_0$. Therefore, if $z^* = z_1 + z_2$, the number of expected contacts, for example is

$$n = N \frac{1}{\sqrt{2\pi\sigma}} \int_d^\infty \exp\left[\frac{-z^{*2}}{2\sigma^2}\right] dz^* \qquad [14]$$

The initial interference and shakedown interference are related to the separation distance by

$$\begin{aligned} \Delta_o &= (z_1 + z_2) - d = z^* - d \\ \delta_o &= (y_1 + y_2) - d = y^* - d \end{aligned} \qquad [15]$$

where y^* is the height variable at shakedown.

From the analysis of the unit event, the mean load per unit length carried over an encounter by two asperities of equal hardness is

$$\frac{\overline{P}}{R_e E^*} = \pi \left[\frac{p_o^s}{R_e E^*}\right]^2 \frac{\delta_o}{\Delta_o}\left[\frac{\Delta_o}{R_e C}\right]\frac{1}{\sqrt{2}} \qquad [16]$$

then, the total expected load is given by

$$\frac{\overline{p}}{R_e E^*} = \frac{\pi}{\sqrt{2}}\left[\frac{p_o^s}{R_e E^*}\right]^2 N \int_d^\infty \frac{\delta_o}{\Delta_o}\left[\frac{\Delta_o}{R_e C}\right]\cdot\Phi(z^*)dz^* \qquad [17]$$

which reduces to

$$\frac{\overline{p}}{R_e E^*} = \left[\frac{p_o^s}{R_e E^*}\right]^2 \frac{N}{\sigma\sqrt{R_e C}} \int_d^\infty X_m(z^* - d)\sqrt{(z^* - d)}\exp\left[\frac{-z^{*2}}{2\sigma^2}\right]dz^* \qquad [18]$$

where $\frac{\delta_0}{\Delta_0} = X_m \sqrt{\frac{4R_e C}{\pi\Delta_0}}$ gives the definition of X_m. The value of X_m is obtained by solving a nonlinear equation given as Eq. [11].

The tangential loading is accounted for only in the shakedown pressure level (p_0^s). This quantity varies with the applied shear traction (Q/P) or with friction. The onset of shakedown is taken to be the point at which the contact pressure equals the shakedown pressure (p_0^s). This value is obtained from the shakedown map for the material and Q/P conditions being studied.[4] The geometry of the contact and the stress-strain description (isotropic *vs* kinematic hardening) influences p_0^s. The normalized shakedown pressure–to–yield stress ratio (p_0^s/k) is 4.0 in the case of $Q/P = 0$. As Q/P increases, the shakedown pressure decreases.[4] In the present case, the shakedown map corresponds to a two-dimensional plane strain analysis of two cylinders in contact. The results for the $Q/P = 0.4$ case are included in Figure 3(b) for comparison with the others.

D. *Determination of Crack Opening Stresses*

An overview of the model is presented in Figure 4(a). As one moves from the top to the bottom figure, the length scale decreases. At the macrolevel (a) the problem is similar to Newman's[30] strip yield model, yet differs significantly in that crack closure results from contact between rough surfaces. The contact stress field S_{contact}, (x), is determined by considering events at lower-size scales. The crack was subdivided into a finite number of strips and the interference in crack surfaces was determined (b). For strip i, many asperities could contact and the load ($\overline{p}$)–displacement relationship is nonlinear. This will be discussed later. This nonlinear behavior is expected, since the contact area gradually increases as the separation between the two surfaces decreases. The load ($\overline{p}$) is the contact stress times the contact (strip) area. The surfaces within strip i can be assumed as Gaussian, exponential, or other distributions. To solve problem (b), the contact of two asperities is analyzed. This analysis of two asperities is shown as (c). In this case, the asperities are crushed by the amount Δ_0 due to relative motion between the upper and lower asperity. The corresponding load-normal displacement relationship between the two asperities is shown as a schematic in (c).

As in Newman's formulation, the crack opening stresses were calculated by solving an elastic problem which, in turn, involved the superposition of two other elastic problems (Figure 4(a)). The first is that of a center crack in a plate, with an advancing crack, $2c$, under uniform far-field stress (S_{appl}), which varies in amplitude between $S_{\max}$ and $S_{\min}$. The second is a partially loaded crack, where the local loading (S_{contact}) is due to contact stresses arising from crack surface interference. Details of this analysis are given later.

The separation distance (d) is equivalent to the crack surface displacement at the strip i; the solution of the contact problem results in S_{contact}. Using superposition and summing the effect all strips, the total crack surface displacement for the ith strip is given by

$$V_i = S_{\text{appl}} \frac{2(1 - \nu^2)}{E}\sqrt{(c^2 - x_i^2)} - \sum_{j=1} S_{\text{contact},j} g(x_i, x_j) \qquad [19]$$

where x_i is the distance to strip i from the origin, ν is Poisson's ratio, E is the elastic modulus, and c is the crack length. In Eq.[19], $g(x_i,x_j)$ is the weight function for a partially loaded crack in an infinite plate and has been determined to be

$$g(x_i,x_j) = G(X_i,x_j) + G(-x_i,x_j) \qquad [20]$$

$$G(x_i,x_j) = \frac{2(1 - \nu^2)}{\pi E}\left[(b - x)\cos h^{-1}\left(\frac{c^2 - bx}{c|b - x|}\right) + \sqrt{c^2 + x^2}\sin^{-1}\left(\frac{b}{c}\right)\right]\Bigg|_{b=b_1}^{b=b_2} \qquad [21]$$

with $b_1 = x_j - w_j$ and $b_2 = x_j + w_j$, where w_j is the width of the jth strip. We note in Eq. [19] that crack surface displacement for the ith strip is dependent on the contact stresses of all strips.

At $S_{\min}$, the contact stresses between the two rough surfaces reach a maximum. Subsequent loading will tend to pull the crack surfaces apart, gradually overcoming the compressive contact stresses. Therefore, the applied stress level at which the contact stresses are overcome is termed the crack opening stress (S_{open}),

$$S_{\text{open}} = S_{\text{appl}} - \sum_{j=1} S_{\text{contact}} \cdot g(x_j) \qquad [22]$$

where $g(x_j)$ is again the appropriate weight function, where

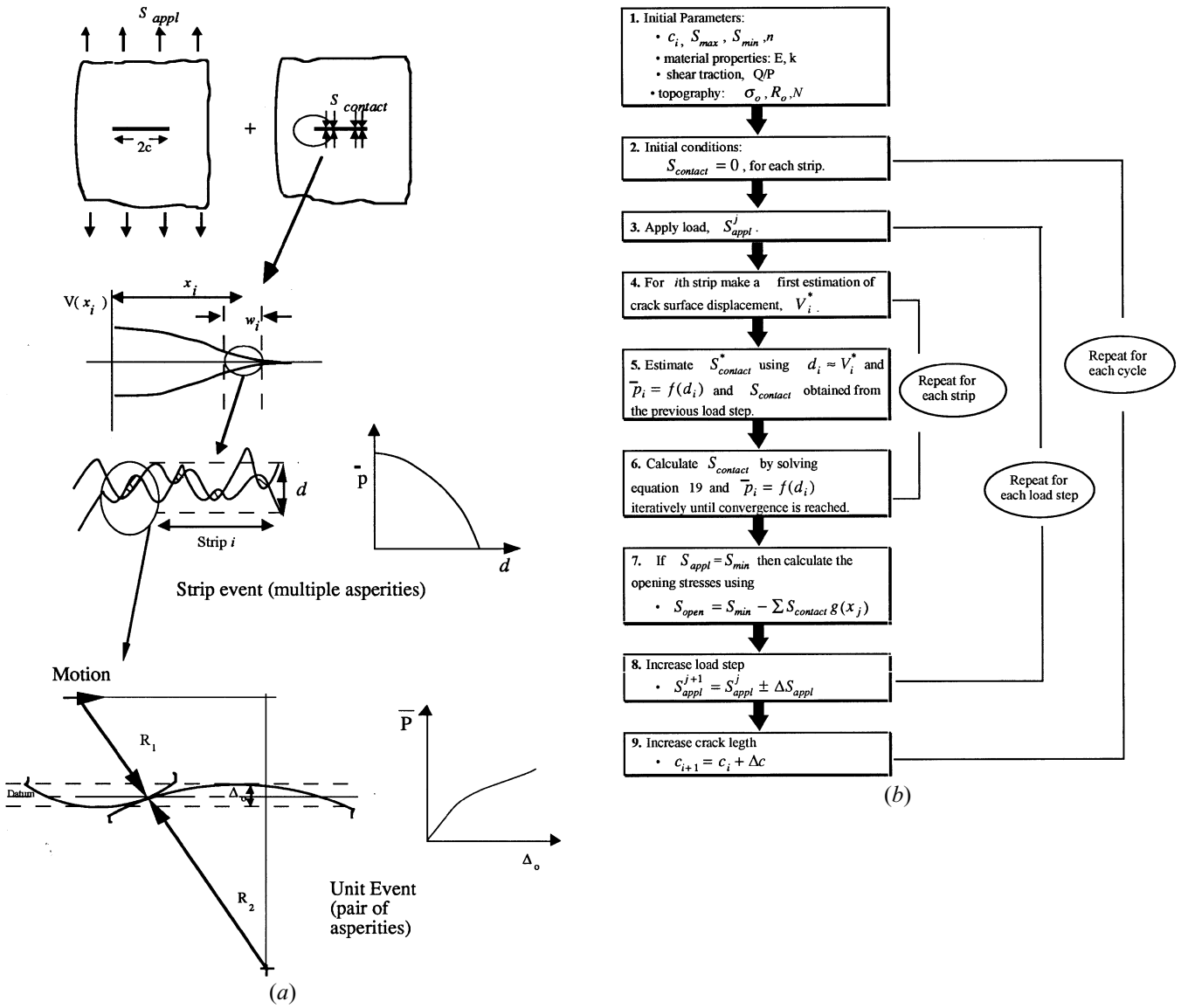

Fig. 4—(*a*) Schematic of the model for crack opening and crack closure. (*b*) Flow chart of the model developed for predicting the crack opening stresses.

$$g(x_j) = \frac{2}{\pi}\left[\sin^{-1}\left(\frac{b_2}{c}\right) - \sin^{-1}\left(\frac{b_1}{c}\right)\right] \qquad [23]$$

III. MODEL IMPLEMENTATION

A. *Description of Algorithm*

An outline of the algorithm developed is shown in Figure 4(b). In the first step within this figure, some parameters are initialized according to the set of conditions to be studied. Initial values for S_{max}, S_{min}, E, k (shear yield stress), and the shear-to-normal traction ratio (Q/P) are assumed, and there are no limitations on the magnitude of these parameters. An initial crack length (c_i) is decided and, furthermore, it is subdivided into a finite number of strips such that the strip width is w_i.

Since the loading cycles began at S_{max}, no contact stresses are present at the beginning of each cycle and initial crack surface displacements were calculated (Eq. [19]). On subsequent load steps the contact stresses are no longer zero. For each strip, the crack displacements at midstrip are made equivalent to the separation distance between contacting surfaces. Therefore, using a curve fit to the appropriate load-separation distance relationship (Figure 3(b), modified KJ), the contact stresses are solved. The analysis was repeated for each load step increment. When the minimum load was reached, the opening stress was calculated using Eq. [22]. After each cycle the crack was advanced by an arbitrary crack-length increment [$(\Delta c/c_i) \approx 0.1$], and the analysis described was repeated for each cycle. Typical simulation time is of the order of a few minutes using a Power Mac (Apple Computer, Cupertino, CA) computer.

The width of each strip (w_i) was kept constant at a value larger than the topographical features so that the statistical considerations held with asperity sizes consistent with reality. At the same time, the strip size should be small enough to allow accurate discretization of crack surfaces at the macrolevel. These considerations usually resulted in an initial number of elements of about ten at the beginning of the simulations. At the end each simulation, typically over 100 strips were analyzed.

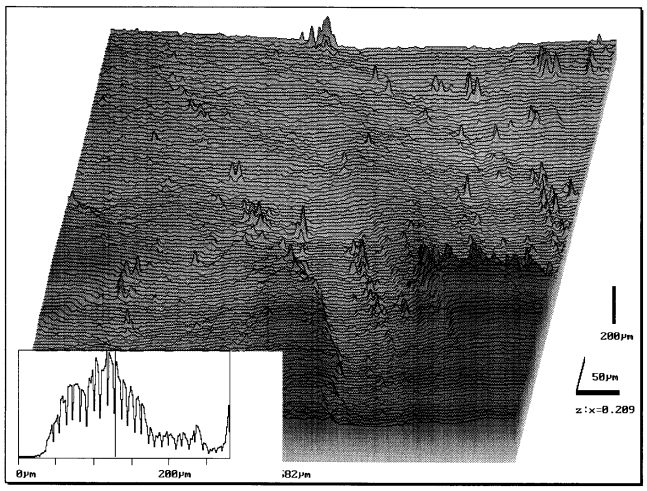

(*a*)

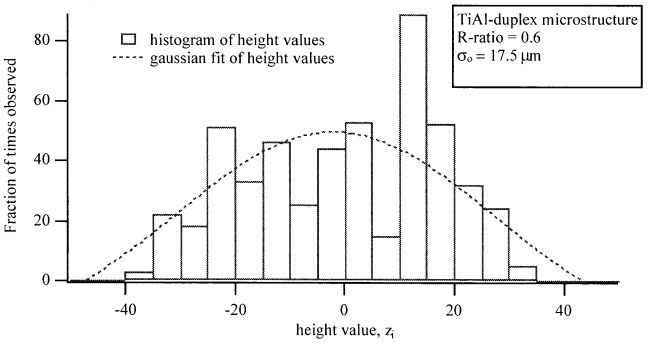

(*b*)

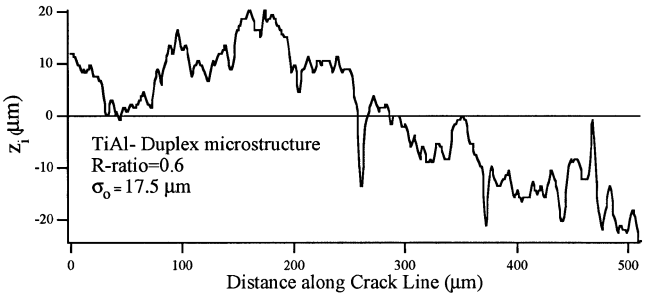

(*c*)

Fig. 5—(*a*) Topographical map of a fully lamellar K5 alloy (γ-TiAl). *R* ratio = 0.1, and σ_0 = 80 μm. (*b*) The histogram of asperity heights for the γ-titanium aluminide. (*c*) The crack profile for the γ-titanium aluminide.

B. *Surface Characterization*

The topography of the fracture surface is described by the following parameters: standard deviation of height for each crack surface (σ_0), asperity tip radius (R_0), and density of asperities (N). The initial standard deviation of asperity heights (σ_0) is assumed to be the same for the two contacting fracture surfaces. Also, for the case $R_1 = R_2 = R_0$, $R_0 = 2R_e$. This accounts, to some degree, for the fact that the surfaces present similar degrees of roughness. We take a reference or datum at $z = 0$, such that the variance is zero, so σ_0 is a function of the height z, given by

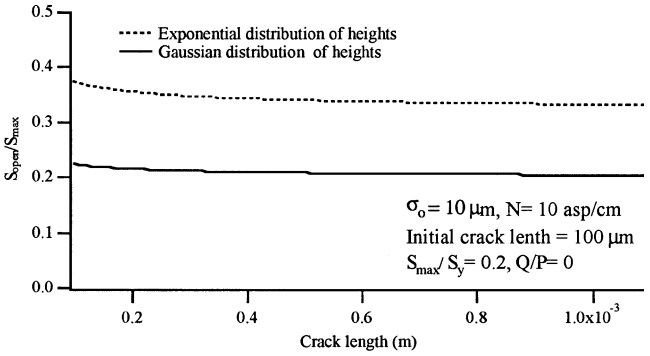

Fig. 6—The role of height distribution in crack opening stresses as a function of crack length.

$$\sigma_o = \left[\frac{\sum_i^n z_i^2}{n-1}\right]^{1/2} \qquad [24]$$

where n is the total number of asperities. The density of asperities (N), *i.e.*, the number of asperities per unit length, is assumed to remain constant over the crack dimension. The initial undeformed radius of asperities tips (R_0) is also assumed constant over the crack dimension. These parameters should be determined experimentally. Surface analysis such as profilometry or confocal microscopy can determine some of these quantities. Confocal microscopy results for a lamellar structure and a histogram of asperity heights for the duplex microstructure of TiAl are shown in Figures 5(a), and (b), respectively. The surface shapes are established by digitizing the three-dimensional profiles. The two-dimensional view of Figure 5(b) is given as Figure 5(c). We note that the value of σ_0 in the duplex case is 17.5 μm, while for the lamellar case it is 80 μm. The distribution chosen is Gaussian and estimates the actual fracture surface profiles. As can be easily observed from the three-dimensional profile of a fracture surface of TiAl in Figure 5(a), the radius varies and should, ideally, be treated as a random variable. This has been left for future studies. The dispersion of asperities (*i.e.*, N) over a given length can be experimentally determined. It is also reasonable to assume that this value does not change through cycling, since while some asperities will be flattened, new ones will make contact.

The resulting opening levels for a Gaussian and exponential distribution of heights are presented in Figure 6. In this simulation, $S_{max}/S_y = 0.2$ and the R ratio is 0.1. Note that in this case, as well as in all future cases, we are using the load-displacement relationship called ''modified KJ.'' The modified KJ for the Gaussian distribution was noted in Figure 3(b) and the response for exponential distribution will differ. In Figure 6, for the case of $\sigma_0 = 10$ μm and an initial crack length of 100 μm, the normalized crack opening stress level was nearly 0.3 for the exponential case and 0.20 for the Gaussian distribution case. This result is somewhat expected, because for the small interference levels the exponential distribution produces higher contact loads. We note that as the crack length increases there is a modest decrease in opening levels. The value of the heights of asperities (σ_0), was assumed to remain constant as the crack grew from 100 to 1000 μm in the simulations.

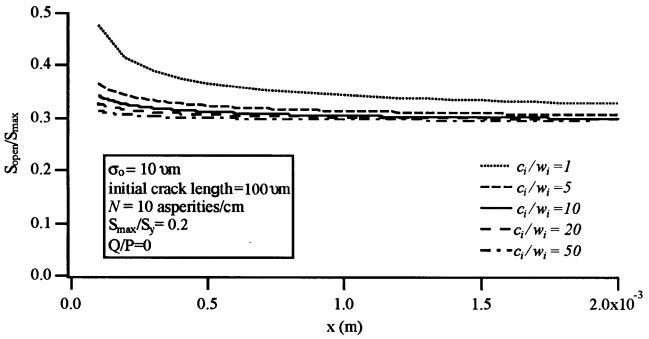

Fig. 7—Crack opening stress *vs* crack length for varying element size.

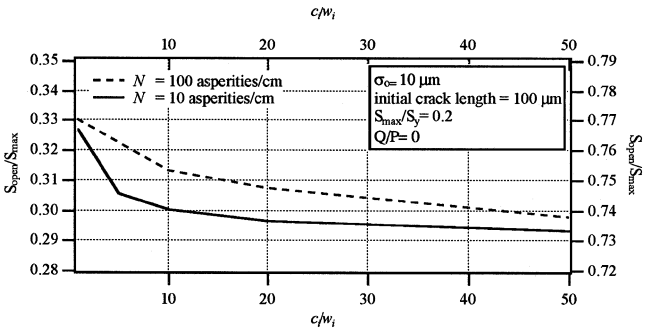

Fig. 8—Normalized opening levels *vs* normalized element size. The opening levels correspond to a crack length of 2.0×10^{-3} m.

C. *Strip Dimensions*

The width of each strip (w_j) should be chosen to permit a statistically significant number of asperities in each strip. As the density decreases, the strip size should be increased to include a large number of asperities for statistical arguments to hold. There have to be limitations on how much this increase should be, because with very large strip sizes the crack surface profile cannot be represented accurately. Therefore, the results point to some optimum number of strips.

Figures 7 and 8 illustrate these points. In Figure 7, the opening levels are grossly overestimated when only one element is considered ($c/w_i = 1$). Clearly, in this case, the crack opening displacements cannot be described correctly either. This is an extreme case, and further discretization lowers the opening levels and collapses the curves, especially at longer-crack lengths.

The trends shown in Figure 8 suggest that as strip sizes become smaller (higher c/w_i), normalized crack opening stress saturates. In Figure 8, simulations are shown for $N = 10$ (solid line) and 100 (dashed line) cases under $S_{max}/S_y = 0.2$. Two observations can be made from this figure. The S_{open}/S_{max} values for the $N = 10$ case approache 0.295 as c/w_i nears 50. But note that the choice of $c/w_i = 10$ gives a normalized opening stress of 0.3, a very close result. For the $N = 100$ case, the normalized opening stress levels are higher and approach 0.735 as c/w_i nears 50. If $c/w_i = 30$ was used in the simulations, this would result in a normalized opening stress of 0.745. Clearly, the strip size should be small enough to accurately characterize the crack profile but at the same time wide enough that statistical treatment of the contact is valid. Therefore, the opening levels in the lower density case ($N = 10$ asperities/cm) begin to reach a plateau value around $c/w_i = 10$, whereas in the higher density case ($N = 100$ asperities/cm), plateau occurs near $c/w_i = 20$.

IV. DISCUSSION OF RESULTS

The current work addresses in detail the role of sliding displacements at crack flanks producing interference, crushing of asperities, and contact pressures. When the crack faces with asperities are displaced in the direction parallel to the crack growth, crack surfaces always come into contact. Depending on the heights of the asperities, the crack surfaces deform plastically before minimum load is reached. The corresponding contact stresses were calculated in this work, and the crack opening stress (S_{open}) required to overcome them was established. Once the crack opening stress is known, it is possible to develop modified driving-force expressions to characterize fatigue crack growth.

The statistical formulation adopted in this study makes some important assumptions that need to be addressed. For one, both fracture surfaces are assumed to be randomly rough, and covariance is ignored. In reality, fracture surfaces are not independent of each other. Mismatch is greatest at the initial stages of crack growth, but it may be partially corrected with plastic deformation as the crack grows, particularly in ductile materials. In the case of sliding contact, not accounting for this covariance may not be as significant. Topographical similarity of fracture surfaces has been partially accounted for in assuming that contacting surfaces present the same asperity height distributions and mean and standard deviations. It is acknowledged that, ideally, covariance should be accounted for, and since some deterministic models[31] are being currently developed, there is the possibility of improving the present model in this aspect. Deterministic contact models can bypass some of these issues. However, they are not as simple and universal as statistical models. They usually demand a full and detailed description of the fracture surface profile, which makes them less attractive. Furthermore, exact matching of surfaces is required, which is very difficult to invoke under repeated loading conditions. Moreover, plasticity is not treated in these models.

The validity of choosing a modified KJ model (Figure 3(b)) for the present problem merits further discussion. The analysis which was developed for the study of wear deals with sliding contact; thus, it is implicit in the derivation of the unit event that each contacting asperity will travel past another. The situation of crack closure is more of a repeated contact between misaligned asperities, which includes both mode I and mode II (normal and sliding) displacements. The interaction of asperities and their profile modification is considered to be due to sliding. In some cases, mode II displacements may not be large enough for the asperities to be displaced past each other. Considering the contact models presented in Figures 1(b) and 3(b), the highest curve corresponds to the original GW elastic analysis. Chang *et al.*[32] predicted lower loads for the same crushing of asperities. Figure 3(b) is a result of KJ's implementation of the JS hard-on-soft asperities analysis. The difference between this curve and the one corresponding to GW with plasticity is a result of accounting for the sliding nature of the individual asperities and, also, the repeated sliding of

the surfaces. In the present work, the KJ analysis was modified using JS's unit event for asperities of equal hardness. This modification accounts for the sliding contact of two randomly rough surfaces. Several requirements should be met before one of these curves (Figure 1(b) and 3(b)) is selected for our analysis. The model must account for deformation history dependence and strain hardening of the material. The fracture surfaces undergo plastic flow, and we note that the profiles are modified most easily by the sliding mode of deformation. Subsequent shakedown in asperities under repeated encounters could produce a profile where the load will be ultimately carried elastically. The modified version of the KJ model, shown in Figure 3(b), satisfies these requirements. The KJ analysis was developed for sliding contact; thus, it is implicit in the derivation of the unit event that each contacting asperity will travel past another. The situation of crack roughness and the misaligned asperities is one that produces both mode I and mode II (normal and sliding) displacements where sliding is dominant for the largest asperities. In the real case, it may be possible that the results could fall between the modified KJ and the Chang *et al.*[32] analysis (its modified version for two deforming asperities of equal hardness). Thus, the use of the modified KJ curve in Figure 3(b) provides a lower bound for contact stresses. This will translate to a slight underestimation of the crack closure levels, and hence, conservative fatigue crack growth predictions.

The extent of the far field tangential loading is controlled by the applied shear loading–to–normal loading ratio (Q/P). This provides flexibility in assessing the closure contribution in different remote loading (mode I/mode II) conditions. The result shown in Figure 3(b) for $p_0^s/k = 2.5$ or $Q/P = 0.4$ (lowest curve) confirms that in the presence of shear loading it is possible to crush the asperities at a lower normal load. For a given Q/P ratio (or friction), the shakedown pressure p_0^s/k is different, as noted in Figure 2(c). This can be established by shakedown theorems of plasticity. Alternately, a cyclic σ-ε analysis of contact can be undertaken establishing the σ-ε loops shakedown to an elastic state.[33] The shakedown limits also change with the geometry of the contact. Lateral *vs* longitudinal asperities, with respect to sliding direction, change the value of p_0^s/k. We note that the shakedown limits for the case of unidirectional sliding were discussed previously. In fatigue loading, the contact surfaces undergo back-and-forward sliding. The underlying stress fields, and hence, the shakedown limits for these two cases, are somewhat different, but the difference is not viewed as significant as far as the current work is concerned. Finally, the problem was greatly simplified by ignoring the through-thickness effects. In reality, the problem is three dimensional. It is likely that mode III displacements are present in a nonflat crack case and the crack surfaces undergo contact in the thickness direction.

The present approach is in agreement with other models' findings, as will be discussed in Part 2 of this article.[1] In his numerical model, Llorca[22] found considerable sensitivity to the crack path description. His description of the rough crack path profile involved two parameters, a tilt angle θ, and a branch length L_p. The tilt angle, which almost solely describes the asperity shape, proved to have a very significant effect on results. Llorca's numerical model predicted closure levels for an aluminum alloy under conditions dominated by roughness effects. For an equivalent asperity height of 10 μm ($\theta = 45$ deg and $L_p = 20$ μm), normalized opening levels (S_{open}/S_{max}) were 0.62 for a 250-μm crack length. By estimating the geometry of the asperity to be about 100 asperities/cm case, the current model predicted $S_{open}/S_{max} = 0.65$ for $S_{max}/S_y = 0.2$ (Part 2 of this article[1]). These results are in agreement with the experimental results of Ritchie *et al.*[34]

The number of asperities during shakedown remains constant, but after shakedown the asperities assume a new height and also a new height distribution. This height distribution is no longer Gaussian. This modified description depends on the nondimensional separation distance d/σ and the nondimensional group $\frac{R_e C}{\sigma}$. In the limiting case (under large contact loads), the asperities are flattened to the same height, and so the distribution approaches a vertical line. If the separation distance between the surfaces is d and the initial interference is Δ_0, after the shakedown is reached the interference is δ_0. Kapoor and Johnson[29] included few examples where they compared the asperity flattening to the experimental results of GW.[25] Similar studies in the context of flattening of asperities in crack growth have not been reported, but represent an area of fruitful research.

Another issue involved with this statistical approach is that a sufficient-length scale must be chosen for strip sizes. It is important to note that from a contact mechanics point of view, the choice is arbitrary; a smaller length can be viewed as covered with smaller asperities, and *vice versa*. However, in the context of fatigue crack propagation, the relevant asperity dimension is related to the material's microstructure. Therefore, asperity size should be on the order of grain size, pearlite colony size, or other microstructural features responsible for the nonlinearity of the crack path. With these considerations, the strip size (width) should be carefully selected. On the other hand, the strip size should be a fraction of the crack length in order to accurately model the crack profile.

V. CONCLUSIONS

1. The work was successful in utilizing statistical contact mechanics concepts to establish the contact stresses and predict the magnitude of asperity-induced closure. The crack opening stress levels produced by the model are in general agreement with experimental observations and with other simplified models. The crack opening stress is both a function of the height of asperities and the density of asperities and is governed by a competition between crack opening displacement and surface profile. Further relations among crack opening stress and other parameters are established in Part 2 of this article.[1]
2. In this analysis of crack closure due to elastic-plastic interaction of asperities on crack surfaces, the JS asperity interaction model was used. This model was chosen because the contact load required to reduce the height of asperities under sliding conditions is lower than the case where no sliding is permitted, and the assumption that asperities will shakedown in the steady state after repeated contact is consistent with reality. The present

treatment permits deformation history dependence, strain hardening, and development of residual stress.

3. The crack closure model is capable of simulating fatigue crack growth of cracks covered with asperities under a broad range of loading conditions. The model can handle R ratio, S_{max}/S_y, and crack length effects. Although simulations were run under constant maximum stress conditions, any other variation in far-field loading can be handled. The numerical implementation of the model is similar to the strip models proposed for plasticity-induced closure, but is fundamentally different because the contact load-displacement relationship is nonlinear.
4. The work considers closure due to crack surface contact, but no plasticity-induced closure effects or oxide-induced closure effects are considered. Plasticity effects are taken into account by permitting the asperities and the fracture surface to deform permanently; however, this interaction of asperities is fundamentally different than the plastic wake effects associated with plasticity-induced closure. The contact stress during the encounter of asperities rises with initial interference following a nonlinear relationship which has been reviewed for several asperity contact models and height distributions.
5. The topographical description of the fracture surfaces is of considerable significance in the prediction of closure levels. For example, the choice of height distribution (Gaussian *vs* exponential) influences the crack opening stress levels, with exponential distribution producing higher S_{open} levels. The work points out the need to include the details of the fracture surface information along with the fatigue crack growth rates, especially in coarse-grained and planar-slip alloys.
6. The strip size–to–crack size ratio influences the crack opening results, but when the number of strips over a crack exceeds 20, the results converge. This result is encouraging, because the number of strips required is not excessive, allowing computation in a very short period. Few runs showed the considerable influence of asperity density on the closure levels for the same level of asperity heights. This will be demonstrated in detail in Part 2 of this article.[1]

ACKNOWLEDGMENTS

The work was sponsored by the Fracture Control Program, College of Engineering, University of Illinois, Urbana. The fractographic analysis and some of the modeling were conducted at Wright Patterson Air Force Base (Dayton, OH), where A. Garcia spent part of Summer 1995. Collaborations with Drs. James Larsen and Brian Worth are acknowledged. The Mathematica software was used in part of the simulations.

NOMENCLATURE

$\Phi(z)$	asperity height probability density function
ΔG	crack length increment
δ_0	shakedown interference
σ_0	standard deviation of heights of a surface
Δ_0	the initial interference between asperities
w_j	width of the jth strip
ν	Poisson's ratio
A	nominal contact area (strip width times the thickness)
C	nondimensional constant, $\left[\frac{p_0^s}{E^*}\right]^2 [2 \ln (4 E^*/p_0^s) - 1]$
c_i	initial crack length
d, d_i	separation distance, separation distance of strip i
E^*	plane strain elastic modulus
GW	Greenwood–Williamson
JS	Johnson–Shercliff
k	yield stress in shear
N	number of asperities per unit length
n	total number of asperities
P	normal load or normal force per unit length for a single asperity (GW model)
$\overline{P}$	average load over a sliding encounter of two asperities (JS model)
$\overline{p}$	total normal load between one or two rough surfaces (GW model)
p_0^s	shakedown pressure
p_0 (x)	maximum Hertzian contact pressure at point x of the sliding contact path
Q/P	tangential traction coefficient
R_e	effective asperity tip radius, $\frac{R_1 R_2}{R_1 + R_2}$
σ	effective standard deviation of asperity heights for two random surfaces in contact, $\sigma = \sqrt{2}\sigma_0$
S_{appl}	far-field stress
$S_{contact}$	contact stress
S_{open}	crack opening stress
S_{max}	far-field maximum stress
S_{min}	far-field minimum stress
S_y	yield stress in tension
V_i	crack surface displacement at midstrip (mode I)
x_h	half-contact width
x_i	distance to strip i from the origin
X_m	x_m/x_e, the ratio of the half-path length of contact at shakedown to the half-path length of elastic contact
z	asperity height
z^*	effective asperity height, $z_1 + z_2$

REFERENCES

1. H. Sehitoglu and A. Garcia: *Metall. Mater. Trans. A*, 1997, vol. 28A, pp. 2277-89.
2. S. Suresh: *Fatigue of Materials*, Cambridge University Press, Cambridge, United Kingdom, 1991.
3. H. Sehitoglu, K. Gall, and A.M. Garcia: *Int. J. Fract.*, 1996, vol. 80 (2–3), pp. 165-92.
4. K.L. Johnson: *Contact Mechanics*, Cambridge University Press, Cambridge, United Kingdom, 1985.
5. N.J. Adams: *Eng. Fract. Mech.*, 1972, vol. 4, pp. 543-54.
6. S. Purushothan and J.K. Tien: *Scripta Metall.*, 1975, vol. 9, pp. 923-26.
7. N. Walker and C.J. Beevers: *Fatigue of Engineering Materials and Structures*, 1979, vol. 1, pp. 135-48.
8. D.L. Davidson and J. Lankford: *Mater. Sci. Eng.*, 1983, vol. 60, pp. 225-29.
9. K. Minakawa and A.J. McEvily: *Scripta Metall.*, 1981, vol. 15, pp. 633-36.
10. J.E. Allison and J.C. Williams: *Titanium Science and Technology*, G. Lujtering, U. Zwicker, and W. Burk, eds., DGM Publishers, Oberusel, 1985, vol. 1, pp. 2243-50.
11. J.M. Larsen: Ph.D. Thesis, Carnegie Mellon University, Pittsburgh,

PA, 1987; also J.M. Larsen, J.C. Williams, and A.W. Thompson: ASTM STP 982, ASTM, Philadelphia, PA, 1988, pp. 149-67.
12. G.T. Gray III, J.C. Williams, and A.W. Thompson: *Metall. Trans. A*, 1983, vol. 14A, pp. 421-33.
13. D. Krueger, S.D. Antolovich, and R.H. Van Stone: *Metall. Trans. A*, 1987, vol. 18A, pp. 1431-49.
14. C.P. Blankenship and E.A. Starke: *Fatigue Fract. Eng. Mater. Struct.*, 1991, vol. 14, pp. 103-14.
15. R.D. Carter, E.W. Lee, E.A. Starke, and C.J. Beevers: *Metall. Trans. A*, 1984, vol. 15A, pp. 555-63.
16. S. Suresh: *Metall. Trans. A*, 1983, vol. 14A, pp. 2375-85.
17. B. Cotterell and J. Rice: *Int. J. Fract.*, 1980, vol. 16, pp. 155-69.
18. S. Suresh and R.O. Ritchie: *Metall. Trans. A*, 1982, vol. 13A, pp. 1627-31.
19. M.C. Smith and R.A. Smith: ASTM STP 924, ASTM, Philadelphia, PA, 1988, pp. 260-80.
20. H. Nakamura and H. Kobayashi: ASTM STP 982, Philadelphia, PA, 1988, pp. 459-74.
21. C.J. Beevers, K. Bell, R.L. Carlson, and E.A. Starke: *Eng. Fract. Mech.*, 1984, vol. 19 (1), pp. 93-100.
22. J. Llorca: *Fatigue Fract. Eng. Mater. Struct.*, 1992, vol. 15 (7), pp. 655-69.
23. R.L. Carlson and C.J. Beevers: *Eng. Fract. Mech.*, 1984, vol. 20, pp. 687-90.
24. J. Tong, J.R. Yates, and M.W. Brown: *Eng. Fract. Mech.*, 1995, vol. 52 (4), pp. 613-23.
25. J.A. Greenwood and J.P.B. Williamson: *Proc. R. Soc.* London, vol. A295, pp. 300-19.
26. S.P. Timoshenko and J.N. Goodier: *Theory of Elasticity*, McGraw-Hill, New York, NY, 1987.
27. J.A. Greenwood and J.H. Tripp: *Proc. Inst. Mech. Eng.*, 1971, vol. 185, pp. 625-33.
28. K.L. Johnson and H.R. Shercliff: *Int. J. Mech. Sci.*, 1992, vol. 34 (5), pp. 375-94.
29. A. Kapoor and K.L. Johnson: *Leeds-Lyon Symp. on Tribology*, 1993, pp. 81-90.
30. J.C. Newman, Jr.: ASTM STP 748, ASTM, Philadelphia, PA, 1981, pp. 53-84.
31. H.A. Francis: *Wear*, 1982, vol. 76, pp. 221-45.
32. W.R. Chang, I. Etsion, and D.B. Bogy: *J. Tribol.*, 1987, vol. 109, pp. 257-63.
33. Y. Jiang and H. Sehitoglu: *Wear*, 1996, vol. 191, pp. 35-44.
34. R.O. Ritchie, W. Yu, A. Blom, and D. Holm: *Fatigue Fract. Eng. Mater. Struct.*, 1987, vol. 10 (5), pp. 343-62.